Diffuse Gamma-Ray Emission from Starburst Galaxies and M31

Item Type	article;article
Authors	Blom, Jan J.;Paglione, Timothy A. D.;Carramiñana, Alberto
Download date	
Link to Item	https://hdl.handle.net/20.500.14394/3404

Diffuse Gamma-Ray Emission from Starburst Galaxies and M31

Jan J. Blom, Timothy A. D. Paglione[1] and Alberto Carramiñana
Instituto Nacional de Astrofísica, Optica y Electrónica, Apartado Postal 216 y 51, 72000
Puebla, Pue., México; blom@inaoep.mx

ABSTRACT

We present a search for high energy gamma-ray emission from 9 nearby starburst galaxies and M31 with the Energetic Gamma-Ray Experiment Telescope (EGRET) aboard the Compton Gamma-Ray Observatory (CGRO). Though the diffuse gamma-ray emission from starburst galaxies was suspected to be detectable, we find no emission from NGC 253, M82 nor from the average of all 9 galaxies. The 2σ upper limit for the EGRET flux above 100 MeV for the averaged survey observations is 1.8×10^{-8} ph cm^{-2} s^{-1}. From a model of the expected radio and $\gamma-$ray emission, we find that the magnetic field in the nuclei of these galaxies is $> 25\mu$G, and the ratio of proton and electron densities is < 400. The EGRET limits indicate that the rate of massive star formation in the survey galaxies is only about an order of magnitude higher than in the Milky Way. The upper limit to the $\gamma-$ray flux above 100 MeV for M31 is 1.6×10^{-8} ph cm^{-2} s^{-1}. At the distance of M31, the Milky Way flux would be over twice this value, indicating higher $\gamma-$ray emissivities in our Galaxy. Therefore, since the supernova rate of the Milky Way is higher than in M31, our null detection of M31 supports the theory of the supernova origin of cosmic rays in galaxies.

Subject headings: cosmic rays — galaxies: starburst — galaxies: individual (NGC 253, M82, M31) — gamma-rays: observations

1. Introduction

To date, the Large Magellanic Cloud (LMC) is the only normal galaxy other than the Milky Way that has been seen in high energy, diffuse $\gamma-$ray emission (Sreekumar et al.

---

[1] also Five College Radio Astronomy Observatory and Department of Physics and Astronomy, Lederle Research Tower, University of Massachusetts, Amherst, MA 01003

1992). Most normal galaxies are simply too distant, and their cosmic ray (CR) densities are too small to have sufficient $\gamma-$ray emissivities. Starburst galaxies, however, have many supernovae due to their unusually high rates of massive star formation. The supernovae produce copious CR electrons seen as bright, extended synchrotron regions (e.g., Seaquist & Odegard 1991; Carilli et al. 1992). In addition, starburst nuclei typically contain high masses of dense molecular gas (Young et al. 1989; Solomon, Downes & Radford 1992; Helfer & Blitz 1993; Paglione et al. 1997). Since CRs are the likely cause of the high temperatures derived deep in the cores of these clouds (Suchkov, Allen & Heckman 1993), $\gamma-$ray production, through interactions between gas and CRs, should be relatively high in starburst galaxies. The challenge has been to accumulate enough exposure time to detect the emission.

As the archetypal starburst galaxies (Rieke et al. 1980), the nearby galaxies NGC 253 and M82 have been the primary targets of $\gamma-$ray searches. Both have high supernova rates of $\sim$ 0.1 yr^{-1} derived from high resolution radio continuum images (van Buren & Greenhouse 1994; Ulvestad & Antonucci 1997). CO maps indicate molecular gas column densities of $\sim 10^{23}\,\mathrm{cm}^{-2}$ within their inner kiloparsec (Paglione et al. 1999; Carlstrom 1989), roughly 10 times that of the Milky Way (e.g. Sanders, Solomon, & Scoville 1984). Studies of their dense molecular gas indicate high average densities of $n_{\mathrm{H}_2} < 3{\times}10^4\,\mathrm{cm}^{-3}$ in M82 to $10^6\,\mathrm{cm}^{-3}$ in NGC 253 (Paglione et al. 1997). Therefore, NGC 253 and M82 are expected to be the brightest starburst galaxies in $\gamma-$rays. However, previous EGRET studies did not detect these objects at high energies (Sreekumar et al. 1994; Paglione et al. 1996).

More CGRO data have become available in the meantime which should improve sensitivity. By some accounts (Pohl 1994), even these starburst galaxies may not be luminous enough in $\gamma-$rays to be detected individually by EGRET with the exposure currently available. However, a combination of all observations obtained for a *collection* of starburst galaxies may add up to a detectable signal. In this paper we present such a search from a survey of 9 nearby starburst galaxies. In addition we analyze $\gamma-$ray observations of the nearby normal galaxy M31.

2. Instrument and Data Analysis

The EGRET spark-chamber on board CGRO operates in the 30 MeV to 30 GeV energy range. The instrument is capable of producing circular γ-ray images with typical radii of 30°. The location accuracy for point sources is about $0\overset{\circ}{.}5$. A detailed description of the instrument and its performance is given by Hughes et al. (1980) and Kanbach et al. (1988). The calibration properties are described by Thompson et al. (1993).

Sky maps are obtained by applying a maximum-likelihood method (Mattox et al. 1996), which provides flux estimates and statistical significances of sources identified in the data. The instrumental background of EGRET is small compared to the measured celestial emission. The celestial background in the EGRET data is dominated by an isotropic component, which is most likely diffuse extragalactic emission (further discussed in Sreekumar et al. 1998). A flat background model which allows for this isotropic emission is created for each observation and energy range. For observations near the Galactic plane, we additionally take into account Galactic diffuse emission by creating models for the HI and CO distributions, and for the inverse-Compton (IC) radiation. These models are made by convolving maps of the gas and photon distributions with an EGRET point-spread function for each energy interval. We apply HI maps based on various 21-cm surveys (combined into an all-sky map; see Bloemen et al. 1986), and the CO map of Dame et al. (1987). The IC distribution is derived from a cosmic ray propagation model by Strong & Youssefi (1995).

We apply the maximum-likelihood analysis software originally developed to analyze data from the COMPTEL γ-ray telescope aboard CGRO. This software has been augmented to analyze archival EGRET data (summarized in Blom 1997), and has been verified to give flux values and significances consistent with published results of the EGRET team.

We use individual archival viewing periods rather than the EGRET all-sky mosaic supplied by the CGRO Science Support Center, because they cover a broader time span (to make our search as sensitive as possible we need the maximum exposure available). The fluxes we derive for several blazar sources near the Galactic plane are consistent with the published EGRET results, which indicates that our diffuse models do not introduce significant deviations. For example, the blazar 2EG J1730-130 at $(l, b) = (12^\circ.03, 10^\circ.81)$ was marginally detected by EGRET above 100 MeV during a two-week pointing in February 1992 at a flux level of $(4.2 \pm 1.5) \times 10^{-7}$ ph cm^{-2} s^{-1} (Thompson et al. 1995), or $(4.4 \pm 1.5) \times 10^{-7}$ ph cm^{-2} s^{-1} based on an improved analysis (Mukherjee et al. 1997). We find $(4.8 \pm 1.5) \times 10^{-7}$ ph cm^{-2} s^{-1}, which is in good agreement with the two flux values published by the EGRET team.

In order to combine different observations for a particular source, we select data from all pointings taken within 30° of the source location and coadd the count distributions and exposure maps separately. The coadding procedure is straightforward only when the viewing periods have matching coordinate systems. The EGRET archives usually provide data in Galactic coordinates when observations are performed near the Galactic plane, otherwise viewing periods are given in equatorial coordinates. For most starburst sources studied in this paper, observations with consistent coordinates are available in the archives. However, in a few cases we are forced to combine data in Galactic coordinates with data in equatorial coordinates. Since we are only interested in the signal at one pixel (the source location), we basically ignore the coordinate system. In other words, we shift the origins of the data sets to the source location and subsequently coadd the files assuming flat coordinates. The same procedure is used to coadd the signals from a *collection* of sources.

Note that we have verified that the mosaics obtained from both coadding procedures are reliable in the sense that analyses of combined blazar observations yield flux values that agree with published results. When we fit a point-source model to combined data at sky locations one or two pixels away from the true source location ($0^\circ.5$ to 1° off), we obtain flux values that are lower than, but consistent with the optimal value. This result shows that our coadding procedure is not sensitive to small coordinate/binning mismatches between viewing periods.

3. Observations and Results

The observation program of CGRO consists of four phases. Phases I to III each consist of ~ 1.5 yr of observations. Phase IV is subdivided into annual cycles, starting with Cycle IV. Data from Phase I up to Phase IV/Cycle V, covering the period 1991–1996, are used in this work. Table 1 shows the relevant EGRET observations for each galaxy in our survey. Specific observing dates of the CGRO phases and viewing periods are given elsewhere (e.g., Gehrels et al. 1994).

The survey consists of ten starburst galaxies selected by distance ($\lesssim 10$ Mpc), IRAS far infrared (FIR) luminosity ($> 10^9\,L_\odot$, Young et al. 1989), and angular distance from the Galactic plane ($b > 10^\circ$). We omit one candidate, NGC 891, because of its proximity to the EGRET source 2EG J0220+4228 (Thompson et al. 1995; Mattox et al. 1997). The large spiral galaxy M31 is analyzed separately as well. Though its FIR luminosity (and therefore the supernova rate) is an order of magnitude lower than a starburst galaxy's, M31 may be close enough to make up for its lower $\gamma-$ray emissivity.

3.1. NGC 253, M82 and M31

All observations listed in Table 1 for NGC 253 and M82 are combined separately. For each source, maximum-likelihood ratio maps are created in six standard EGRET energy ranges (70–100 MeV, 100–150 MeV, 150–300 MeV, 300–500 MeV, 0.5–1 GeV, and 1–2 GeV), and in one broad energy range covering all photon energies > 100 MeV. Flux values are derived by simultaneously fitting point-source models at the locations of the starburst galaxy and all respective neighboring EGRET catalog sources within 25° on the sky (Thompson et al. 1995, 1996).

None of the likelihood maps show evidence for emission from NGC 253 or M82. Upper limits (2σ) obtained from model fitting are shown in Figure 1. Note that no upper limit is derived for M82 at 1–2 GeV due to limited statistics. For NGC 253 we find a 2σ upper limit to the γ−ray emission above 100 MeV of 3.4×10^{-8} ph cm^{-2} s^{-1}. For M82 this limit is 4.4×10^{-8} ph cm^{-2} s^{-1}. Note that both limits are well below previous estimates (Sreekumar et al. 1994; Paglione et al. 1996), which further constrains emission models (§4).

We apply the same analysis technique for M31 at > 100 MeV only. No evidence for M31 is found in this energy range. We find a 2σ upper limit for the flux above 100 MeV of 1.6×10^{-8} ph cm^{-2} s^{-1}. This value is below the estimate of Özel & Berkhuijsen (1987).

3.2. Combining All Available Starburst Galaxy Observations

In order to create a "supermosaic" for all starburst galaxies listed in Table 1, the observations for each source are first combined separately. The resulting submosaics are then coadded such that the locations of all starburst galaxies match in one pixel (with arbitrary coordinates). In addition, the event distributions of the submosaics are scaled to ensure that each starburst galaxy contributes equally in exposure to the supermosaic. All background models are treated similarly.

We create maximum-likelihood ratio images for the supermosaic in six standard EGRET energy ranges between 70 MeV and 2 GeV, and for all photon energies > 100 MeV. These images show significant excesses that can be identified with the source signals of strong EGRET blazars which remain visible in the supermosaic even after adding noise from observations that do not contain these sources. However, no evidence for γ−ray emission at the shared location of the starburst galaxies is found. Upper limits derived from simultaneous model fitting taking the EGRET blazars into account are shown in the right panel of Figure 1. The 2σ upper limit we derive for the *average* γ−ray emission above 100 MeV from starburst galaxies is 1.8×10^{-8} ph cm^{-2} s^{-1}.

4. The Expected Gamma-Ray Emission from Starburst Galaxies

To calculate the γ−ray flux from a starburst galaxy, we model the CR production and radiation mechanisms for NGC 253 and M82. A full description of the model is given in Paglione et al. (1996). In short, we assume a power law form for the initial CR injection spectrum $Q = KE^{-s}$, and allow it to evolve to a steady state. The ambient density (with a main contribution from H_2 in galactic nuclei), magnetic field and photon field determine the energy loss rates due to bremsstrahlung, synchrotron and IC radiation, as well as secondary particle production. The model yields steady state primary and secondary electron, and proton energy distributions, which are used to calculate synchrotron and $\gamma-$ray spectra. The normalization of the proton injection spectrum is estimated by comparing the modeled and observed synchrotron radio spectra. This normalization corresponds to the total power per unit time transferred by supernovae into cosmic rays within a given volume,

$$\int_{E_{min}}^{\infty} QE \; dE = \eta P \Psi / V \quad . \tag{1}$$

Here η is the efficiency of energy transfer from a supernova to CRs, $P \approx 10^{51}$ ergs is the supernova energy, Ψ is the supernova rate, and V is the volume. Solving for the normalization K, we find (for a minimum energy E_{min} and a power law slope of 2.2),

$$K = \frac{\eta P \Psi}{V} 0.2 \; E_{min}^{0.2} \quad . \tag{2}$$

A minimum CR energy, $E_{min} \gtrsim 2 m_p v_s^2$ (Bell 1978), is required for acceleration in a shock front. It is roughly a few MeV for a shock velocity of $10^4 \,\mathrm{km\,s^{-1}}$. To generate $\gamma-$ray fluxes, the model results are integrated over volume and divided by $4\pi D^2$, where D is the galaxy distance.

4.1. NGC 253 and M82

For NGC 253, we choose a disk-shaped starburst region 70 pc thick, with a radius of 325 pc (Paglione et al. 1999), and $\Psi = 0.08$ yr^{-1} (Ulvestad & Antonucci 1997). For M82, $\Psi = 0.1$ yr^{-1} (van Buren & Greenhouse 1994), and the disk is 50 pc thick with a radius of 355 pc (Shen & Lo 1995). Paglione et al. (1996) tested for $\gamma-$ray emission outside the starburst region and found it to be negligible, so we ignore any interactions outside the nucleus. The calculated synchrotron spectra resulting from the model CR electron distributions match the shape of the observed radio spectra from the nuclei of NGC 253 and M82 (Carilli 1996; Carlstrom & Kronberg 1991) given a photon field of 200 $\mathrm{eV\,cm^{-3}}$ and a diffusion time scale of 10 Myr (cf. Paglione et al. 1996). The average gas densities for NGC 253 and M82 are 300 and 100 cm^{-3}, respectively. Emission measures of $\sim 3{\times}10^5$ and 10^6 cm^{-6} pc are required to match the free-free component and thermal absorption (low frequency turn-over) of the spectra from NGC 253 and M82, respectively (cf., Carilli 1996; Carlstrom & Kronberg 1991).

On the whole, the density and photon field are well constrained by the radio spectra. The density range is limited by the slope of the radio spectrum. Higher densities increase the CR losses due to collisions with matter, thus reducing the number of low energy CRs, resulting in a flatter synchrotron spectrum. (Note that thermal absorption only affects the spectrum at low frequencies and is easily distinguished from the inherent slope of the underlying emission.) The volume-averaged densities that best match the radio spectra agree well with those found from molecular line studies (Paglione et al. 1997). The photon field is determined by the FIR luminosity and, to a much lesser degree, by the synchrotron slope. A steeper slope indicates a higher photon field since more high energy electrons are lost due to IC radiation.

The absolute level of the model synchrotron spectrum is determined by the magnetic field B, the ratio of proton and electron densities N_p/N_e, and η. Though the magnetic field, derived from radio data, is most likely $\gtrsim 50\mu$G in NGC 253 and M82 (Carilli 1996; Seaquist & Odegard 1991), N_p/N_e and η are unknown. The N_p/N_e ratio can be anywhere between 20 and 2000, though values of 50 to a few hundred appear most likely for the Milky Way (Bell 1978). Values for the efficiency of energy transfer between 10 and 50% have been found from models of the evolution of supernova blast waves (Markiewicz, Drury & Völk 1990). Fortunately, the $\gamma-$ray flux depends only very weakly on B and N_p/N_e. Therefore, η is the most important parameter needed to predict the $\gamma-$ray flux, and it is determined from the radio spectrum normalization.

Five models (A–E, Table 2) are shown with the EGRET upper limits in Figure 1. The $\gamma-$ray spectra are summations of IC, bremsstrahlung and neutral pion decay radiation. Near 100 MeV, the emission is dominated by neutral pion decays as seen by the so-called "pion bump." Though all the models lie below the M82 limits, model A predicts a $\gamma-$ray flux above 100 MeV for NGC 253 higher than measured.

4.2. Starburst Galaxy Survey

From their integrated radio spectra and molecular gas properties, the other galaxies in the survey are relatively similar to NGC 253 and M82. We assume that the major difference in the normalization between starburst galaxies is the supernova rate and distance (Equation 2). We estimate the supernova rate from the FIR luminosity (van Buren & Greenhouse 1994). For NGC 4945, a starburst with very high gas densities (Jackson et al. 1995), we use the model fit to NGC 253. For the other starburst galaxies, we use the model for M82. The expected average $\gamma-$ray spectra from models A–E are shown in Figure 1 with the EGRET upper limits. Unlike the models for NGC 253, which are constrained by the

EGRET points near the pion bump, these results are limited by the data near 1 GeV.

5. Discussion

Though many of the model fluxes lie below the EGRET limits, all but one or two models may be eliminated. The low magnetic field in model A contradicts minimum energy estimates from radio data (Beck et al. 1994; Rieke et al. 1980). Models A and B both have very high transfer efficiencies, and their $\gamma-$ray spectra are above or very near near the 2σ limits in a few energy bands for NGC 253 and the starburst galaxies. With model B eliminated, we conclude that $N_p/N_e < 400$, as in the Milky Way. Note that model B may still be valid for M82, though we have no reason to believe that the CR population would be so different in this particular galaxy.

The magnetic field used for model C agrees with previous calculations, and the N_p/N_e ratio of 100 matches that observed for the Milky Way near 1 GeV. The integrated fluxes and spectra all fall below the EGRET limits.

After reviewing the calculation of the minimum energy magnetic field, we find model D to be a poor solution. From the equation for magnetic field strength in Beck et al. (1994), we find a gas volume filling factor in NGC 253 of $\sim 5{\times}10^{-3}$ for model D. This result implies ionized cloud densities of roughly $10^{4.5}\,\mathrm{cm}^{-3}$. Since these densities approach those found for the dense molecular medium in NGC 253 (Paglione et al. 1999), model D may not be appropriate due to its low volume filling factor. Assuming similar magnetic fields in M82 and the starburst galaxies, model D is most likely not valid for them either.

Another argument against model D comes from comparing its predictions with the expected Milky Way flux. The $\gamma-$ray luminosity of the Milky Way measured by EGRET above 100 MeV is roughly $2{\times}10^{42}$ ph s^{-1} (S. Hunter, private communication), and its FIR luminosity is $7{\times}10^{9}\,L_{\odot}$ (Cox & Mezger 1989). When we scale the Milky Way $\gamma-$ray luminosity to the average starburst FIR luminosity (which is roughly 4 times higher) and distance (7.4 Mpc), we would observe a $\gamma-$ray flux of $F_{\gamma}(E > 100\,\mathrm{MeV}) \sim 1.3{\times}10^{-9}$ ph cm^{-2} s^{-1}. This is nearly the flux predicted for the survey sources with model D. Since the $\gamma-$ray emissivity should be higher in starburst galaxies due to their larger average gas densities, this simple scaling most likely underestimates the true flux. We therefore consider model D at best a lower limit prediction.

Model E is eliminated since the predicted fluxes all fall below the scaled estimate from the Milky Way. Further, the $\gamma-$ray flux of the LMC (Sreekumar et al. 1992), when similarly scaled, is consistent with, or slightly above, the fluxes from model E. The $\gamma-$ray emissivity of the LMC is much lower than in starburst galaxies. At a distance of 50 kpc, even the $\gamma-$ray flux of the Milky Way is already 35 times higher than in the LMC. Therefore, the fluxes predicted by model E are clearly too low. Note that this result does not strictly eliminate $N_p/N_e \leq 50$ – with this ratio we can obtain fluxes that are similar to model D given $\eta = 0.13$ and $B = 50\mu$G.

Based on our new analysis and EGRET limits, we expect the flux estimates from model C to be the most realistic (with model D as a lower limit). These models imply $N_p/N_e < 400$, similar to the Galactic value for CR energies $\gtrsim$1 GeV. The energy from supernovae is also efficiently transferred to CRs ($\eta \sim$ 20–50%). The survey sources have magnetic field strengths $> 25\,\mu$G.

The EGRET limits also constrain the relative supernova (or massive star formation) rate in the starburst galaxies. At the average distance of our survey sources, the flux above 100 MeV from the Milky Way would be $3{\times}10^{-10}$ ph cm^{-2} s^{-1}. Compared with the observed starburst upper limit, we find $\Psi_{SBG}/\Psi_{MW} < 60$. This limit is conservative since not even a hint of starburst emission is found in the EGRET maps. The integrated fluxes from models C and D indicate $\Psi_{SBG}/\Psi_{MW} \lesssim 20$ and the difference in FIR luminosities implies $\Psi_{SBG}/\Psi_{MW} \gtrsim 4$. Given the uncertainties in η, we estimate that the star formation rate in starburst galaxies is only about an order of magnitude higher than in the Milky Way. Studies at other wavelengths also indicate star formation rates elevated by this magnitude (e.g., Kennicutt 1998).

5.1. M31 and the Supernova Origin of Cosmic Rays

It is interesting to note that at the distance of M31, the flux of the Milky Way above 100 MeV would be $4{\times}10^{-8}$ ph cm^{-2} s^{-1}. This flux is over twice the EGRET limit for M31. Therefore, the Galactic $\gamma-$ray emissivity must be higher than in M31. Three main differences between our Galaxy and M31 can explain this result. First, the supernova rate in the Milky Way is roughly 7 times higher than in M31, as can be estimated from the FIR luminosity. This difference is probably even more pronounced because much of the FIR emission in M31 originates from Population II stars in the nucleus rather than from massive star forming regions (Dame et al. 1993). Therefore, if CRs are in fact accelerated in the shock fronts of supernovae, the CR density in the Milky Way, and thus its $\gamma-$ray emissivity, should be higher. Second, the mass of H I and H_2 in the Milky Way is at least 6 times that of M31 (e.g., Dame et al. 1993; Clemens, Sanders & Scoville 1988). Third, unlike the starburst galaxies and the Milky Way, M31 lacks a massive concentration of dense molecular gas in its nucleus (though some unexplained radio emission is seen there). This implies a lower secondary particle production in M31 (including neutral pions) which means a lower diffuse $\gamma-$ray flux. However, the $\gamma-$ray emissivity does not depend very strongly on density, so the difference in supernova rates is the most important factor determining the high energy emission from galaxies. We conclude that our null detection of hard $\gamma-$ray emission from M31, compared with the predicted Milky Way flux at the same distance, supports the theory of the supernova origin of CRs.

5.2. Possible Point-source Contributions

Throughout the paper we have neglected point-source contributions to the high-energy emission from starburst galaxies, M31, and the Milky Way. In principle, a large population of relatively weak $\gamma-$ray sources may add significantly to the total high-energy emission of a galaxy. Studies on the nature of the many unidentified EGRET sources suggest that supernova remnants (without an embedded pulsar), X-ray binaries and flare stars are all possible, but not yet well-established sources of high-energy $\gamma-$rays (Mukherjee, Grenier & Thompson 1997). Pulsars are the only firmly identified small-scale objects that are known to emit $\gamma-$rays up to GeV energies. Therefore, we calculate the $\gamma-$ray emission from a Galactic ensemble of pulsars to estimate the possible contribution of such a source population to the overall $\gamma-$ray luminosity in a galaxy.

EGRET has detected 7 pulsars above 100 MeV in the Galaxy which show an increasing efficiency in converting rotational energy of the spinning neutron star into $\gamma-$rays versus pulsar age. A second obvious trend is an increasing spectral hardening in the $\gamma-$ray regime versus age (Fichtel & Trombka 1997). Their typical pulsed $\gamma-$ray spectra can be described by power-laws which cut off or break at 1–10 GeV (Thompson et al. 1997). All *radio* pulsars in the (fairly complete) Princeton Pulsar catalog (Taylor, Manchester & Lyne 1993) may generally have similar $\gamma-$ray emission properties. When we assume that the radio and $\gamma-$ray emission cones of pulsars have the same aperture, we can easily estimate an integrated pulsar contribution to the high-energy emission of the Galaxy above 100 MeV. We find a maximum contribution of 2% when we adopt a long-lived pulsar activity ($\sim 10^7$ yr) and an average spectral cut-off at low $\gamma-$ray energies ($\sim$ 2 GeV). This result indicates that pulsars add an insignificant fraction to the total $\gamma-$ray luminosity of the Galaxy above 100 MeV. This is in agreement with the findings of Pohl et al. (1997), who conclude that only for energies > 1 GeV we may find a significant contribution (up to 18%) in selected sky regions.

The flux values listed in the EGRET catalogs imply that the integrated $\gamma-$ray emission from unidentified sources is comparable to that from pulsars. If all the EGRET unidentifieds are Galactic sources of some type other than pulsars (which is in fact unlikely), then we have a maximum total point-source contribution of 4% to the overall emission > 100 MeV in the Galaxy. Since we have no reason to expect a more dominant contribution from pulsars (and other point sources) in starburst galaxies or M31, we conclude that it is justified to neglect point-source contributions in our model predictions.

6. Conclusions

Our combined EGRET observations are the most sensitive measurements of starburst galaxies ever performed at hard $\gamma-$ray energies. However, no MeV or GeV emission from starburst galaxies is identified. Nevertheless, we have shown that the derived EGRET upper limits are useful for constraining models of CR and $\gamma-$ray production in galaxies. The modeling implies large average gas densities, magnetic fields, and photon fields. We find $50 \lesssim N_p/N_e < 400$, similar to the Milky Way value, and a high efficiency of energy transfer from supernovae to CRs (20–50%). These values agree well with radio observations.

The $\gamma-$ray emissivity of M31 is at most half that of the Milky Way. This result supports the supernova origin of CRs because of the lower supernova rate of M31.

According to our model predictions, an instrument with an order of magnitude better sensitivity than EGRET should be able to detect NGC 253 and M82 in a one-year all-sky survey. The Gamma-ray Large Area Space Telescope (GLAST; e.g., Michelson 1996), with a projected point-source sensitivity in one year of $5{\times}10^{-9}$ ph cm^{-2} s^{-1}, may have this capability. The GLAST pair conversion telescope is being designed to image the 10 MeV – 300 GeV sky. Its launch is expected in the first decade of the next century.

This research has made use of the NASA/IPAC Extragalactic Database (NED) which is operated by the Jet Propulsion Laboratory, Caltech, under contract with the National Aeronautics and Space Administration. J. J. B. acknowledges computational support from the Space Research Organization Netherlands (SRON) in Utrecht, The Netherlands. We thank S. Bloom and S. Hunter for helpful discussions.

REFERENCES

Beck, R., Carilli, C. L., Holdaway, M. A., Klein, U. 1994, A&A, 292, 409

Bell, A. R. 1978, MNRAS, 182, 443

Bloemen, J. B. G. M., Strong, A. W., Mayer-Hasselwander, H. A., et al. 1986, A&A, 154, 25

Blom, J. J. 1997, Ph. D. Thesis, Univ. of Leiden, The Netherlands, Appendix B

Carilli, C. L. 1996, A&A, 305, 402

Carilli, C. L., Holdaway, M. A., Ho, P. T. P., & De Pree, C. G. 1992, ApJ, 399, L59

Carlstrom, J. E. 1989, Ph. D. Thesis, Univ. of California, Berkeley

Carlstrom, J. E. & Kronberg, P. P. 1991, ApJ, 366, 422

Clemens, D. P., Sanders, D. B., & Scoville, N. Z. 1988, ApJ, 327, 139

Cox, P. & Mezger, P. G. 1989, A&A Rev., 1, 49

Dame, T., Koper, E., Israel, F. P., Thaddeus, P. 1993, ApJ, 418, 730

Dame, T., Ungerechts, H., Cohen, R. S. et al. 1987, ApJ, 322, 706

Fichtel, C. E. & Trombka, J. I. 1997, in Gamma-Ray Astrophysics, New Insight Into the Universe, 2nd edition, NASA ref. pub. 1386, 148-149

Gehrels, N., Chipman, E., Kniffen, D. A., 1994, in Proc. Second Compton Symposium, eds. C. E. Fichtel et al., AIP Conf. Proc. 304, 3

Helfer, T. T. & Blitz, L. 1993, ApJ, 419, 86

Hughes, E. B., Hofstadter, R., Johansson, A. et al. 1980, IEEE Trans. Nucl. Sci., NS-27, 364

Jackson, J. M., Paglione, T. A. D., Carlstrom, J. E., & Rieu, N. -Q. 1995, ApJ, 438, 695

Kanbach, G. Bertsch, D. L., Fichtel, C. E. et al. 1988, Space Sci. Rev., 49, 69

Kennicutt, R. C., Jr. 1998, ApJ, 498, 541

Markiewicz, W. J., Drury, L. O'C., Völk, H. J. 1990, A&A, 236, 487

Mattox, J. R., Bertsch, D. L., Chiang, J. et al. 1996, ApJ, 461, 396

Mattox, J. R., Schachter, J., Molnar, L., Hartman, R. C., Patnaik, A. R. 1997, ApJ, 481, 95

Michelson, P. F. 1996, Gamma-Ray and Cosmic-Ray Detectors, Techniques, and Missions, B. D. Ramsey, T. A. Parnell, Eds., Proc. SPIE, 2806, 31

Mukherjee, R., Bertsch, D. L., Bloom, S. D. et al. 1997, ApJ, 490, 116

Mukherjee, R., Grenier, I. A. & Thompson, D. J. 1997, in Proc. Fourth Compton Symposium, eds. C. D. Dermer et al. AIP Conf. Proc. 410, Part 1, 394

Özel, M. E. & Berkhuijsen, E. M. 1987, A&A, 172, 378

Paglione, T. A. D., Jackson, J. M., & Ishizuki, S. 1997, ApJ, 484, 656

Paglione, T. A. D., Marscher, A. P., Jackson, J. M., & Bertsch, D. L. 1996, ApJ, 460, 295

Paglione, T. A. D., Yam, O., Jackson, J. M., & Tosaki, T. 1999, submitted to ApJ

Pohl, M. 1994, A&A, 287, 453

Pohl, M., Kanbach, G., Hunter, S., Jones, B., ApJ, 491, 159

Rice, W., Lonsdale, C. J., Soifer, B. T., Neugebauer, G., Kopan, E. L., Lloyd, L. A., de Jong, T., Habing, H. J. 1988, ApJS, 68, 91

Rieke, G. H., Lebofsky, M. J., Thompson, R. I., Low, F. J., & Tokunga, A. T. 1980, ApJ, 238, 24

Sanders, D. B., Solomon, P. M., & Scoville, N. Z. 1984, ApJ, 276, 182

Seaquist, E. R. & Odegard, N. 1991, ApJ, 369, 320

Shen, J. & Lo, K. Y. 1995, ApJ, 445, L99

Solomon, P. M., Downes, D. & Radford, S. J. E. 1992, ApJ, 387, L55

Sreekumar, P. et al. 1992, ApJ, 400, L67

Sreekumar, P. et al. 1994, ApJ, 426, 105

Sreekumar, P. et al. 1998, ApJ, 494, 523

Strong, A. W., Youssefi, G. 1995, Proc. 24th ICRC, 3, 48

Suchkov, A., Allen, R. J. & Heckman, T. M. 1993, ApJ, 413, 542

Taylor, J. H., Manchester, R. N. & Lyne, A. G. 1993, ApJS, 88, 529

Thompson, D. J., Bertsch, D. L., Fichtel, C. E. et al. 1993, ApJS, 86, 629

Thompson, D. J., Bertsch, D. L., Dingus, B. L. et al. 1995, ApJS, 101, 259

Thompson, D. J., Bertsch, D. L., Dingus, B. L. et al. 1996, ApJS, 107, 227

Thompson, D. J., Harding, A. K., Hermsen, W. & Ulmer M. P., 1997, in Proc. Fourth Compton Symposium, eds. C. D. Dermer et al. AIP Conf. Proc. 410, Part 1, 39

Ulvestad, J. S. & Antonucci, R. R. J. 1997, ApJ, 488, 621

van Buren, D. & Greenhouse, M. A. 1994, ApJ, 431, 640

Young, J. S., Xie, S., Kenney, J. D. P., and Rice, W. L. 1989, ApJS, 70, 699

This preprint was prepared with the AAS LaTeX macros v4.0.

Fig. 1.— The expected $\gamma-$ray flux from (left to right) NGC 253, M82 and the starburst galaxies (SBGs), shown with the EGRET 2σ upper limits (dots). Model parameters are listed in Table 2.

Table 1. Starburst Galaxies and EGRET Observations.

Galaxy	D (Mpc)	l	b	L_{FIR} ($10^{10}\,L_\odot$)	CGRO Viewing Periods
M31	0.67	121°.1	−21°.6	0.1[a]	26.0, 28.0, 34.0, 37.0, 211.0, 325.0, 401.0, 425.0, 530.0 **Total Exposure:** 0.6×10^9 cm^2 s
IC 342	1.8	138.2	10.6	0.2	15.0, 18.0, 31.0, 211.0, 216.0, 319.0, 319.5, 325.0, 401.0, 411.0, 411.5, 518.5, 530.0 **Total Exposure:** 1.3×10^9 cm^2 s
M82	3.25	141.4	40.6	3.2	18.0, 22.0, 216.0, 227.0, 228.0, 319.0, 319.5, 411.0, 411.5, 418.0, 518.5 **Total Exposure:** 1.8×10^9 cm^2 s
NGC 253	3.4	97.4	−88.0	2.8	9.0, 13.5, 404.0, 428.0 **Total Exposure:** 0.6×10^9 cm^2 s
M83	5.4	314.6	32.0	2.0	12.0, 23.0, 32.0, 207.0, 208.0, 215.0, 217.0, 316.0, 405.0, 405.5, 408.0, 424.0, 511.5 **Total Exposure:** 1.1×10^9 cm^2 s
NGC 2903	7.0	208.7	44.5	0.8	40.0, 322.0, 326.0, 403.5 **Total Exposure:** 0.6×10^9 cm^2 s
NGC 4945	7.0	305.3	13.3	8.5[a]	12.0, 14.0, 23.0, 27.0, 32.0, 207.0, 208.0, 215.0, 217.0, 230.5, 303.0, 314.0, 315.0, 316.0, 402.0, 402.5, 424.0, 522.0, 531.0 **Total Exposure:** 1.4×10^9 cm^2 s
M51	9.7	104.8	68.6	3.1	4.0, 22.0, 218.0, 222.0, 418.0, 515.0 **Total Exposure:** 0.6×10^9 cm^2 s
NGC 6946	11.0	95.7	11.7	4.8	2.0, 34.0, 203.0, 212.0, 302.0, 303.2, 303.7, 318.1, 401.0, 530.0 **Total Exposure:** 0.9×10^9 cm^2 s
NGC 3628	11.5	169.4	13.9	1.9	3.0, 4.0, 11.0, 204.0, 205.0, 206.0, 222.0, 304.0, 305.0, 306.0, 307.0, 308.0, 308.6, 311.0, 311.6, 312.0, 313.0, 322.0, 326.0, 511.0, 515.0 **Total Exposure:** 1.2×10^9 cm^2 s

[a] Adapted from Rice et al. (1988)

Table 2. Parameter values for starburst emission models.

Model	B	N_p/N_e	η	$F(E > 100\,\mathrm{MeV})$ 10^{-9} ph cm^{-2} s^{-1}		
	(μG)			NGC 253	M82	SBGs
A . . .	25	50	0.90	36.5	37.5	14.4
B . . .	50	400	0.73	24.1	27.6	10.0
C . . .	50	100	0.43	15.6	16.7	6.3
D . . .	100	100	0.15	5.3	6.1	2.2
E . . .	100	50	0.05	2.0	2.2	0.8

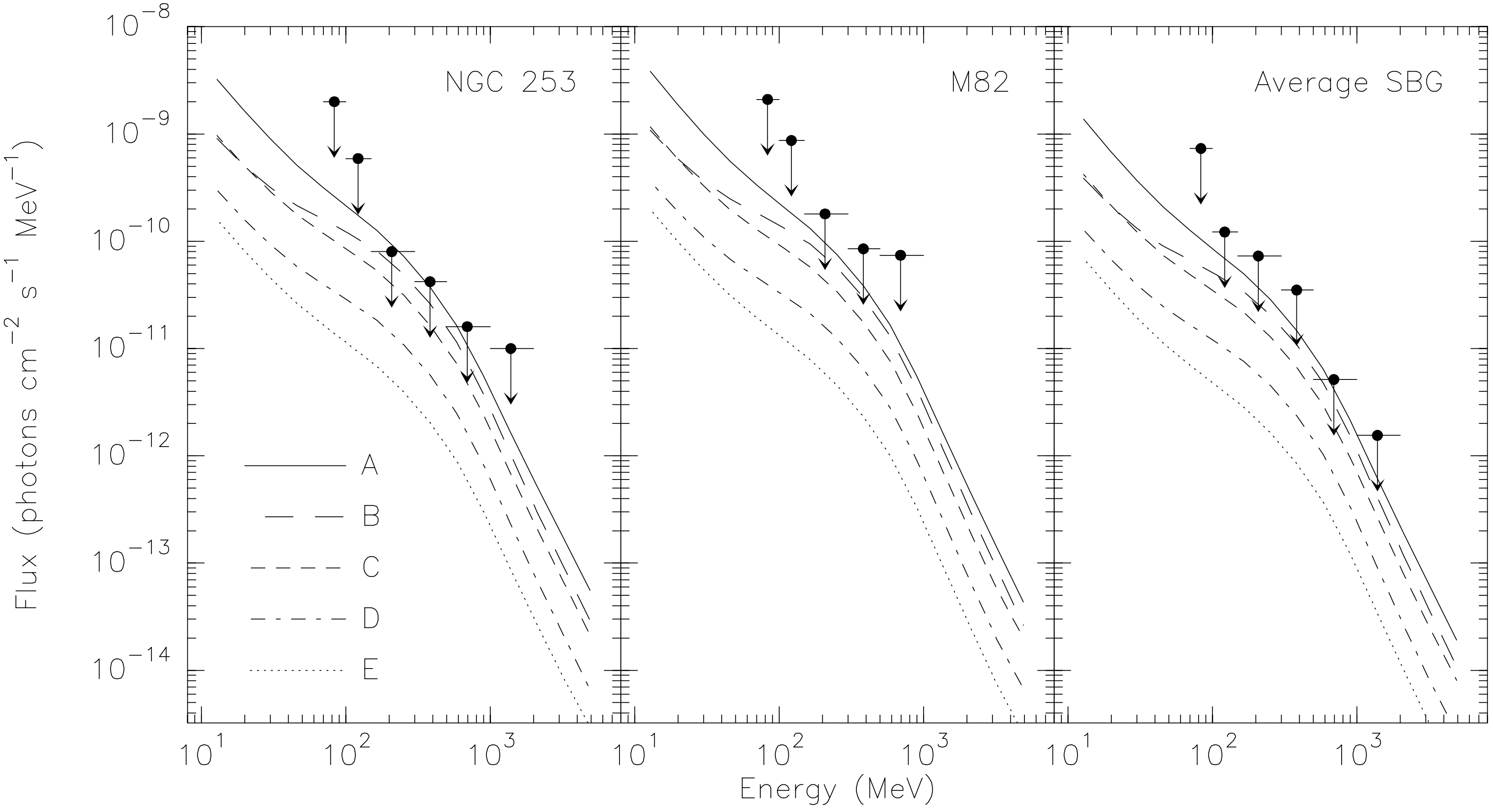

NGC 253
M82
Average SBG
A
B
C
D
E
Flux (photons cm^{-2} s^{-1} MeV^{-1})
10^{-8}
10^{-9}
10^{-10}
10^{-11}
10^{-12}
10^{-13}
10^{-14}
10^{1}
10^{2}
10^{3}
Energy (MeV)